AAS 07-201

NON-PARAMETRIC COLLISION PROBABILITY FOR LOW-VELOCITY ENCOUNTERS

J. Russell Carpenter*

An implicit, but not necessarily obvious, assumption in all of the current techniques for assessing satellite collision probability is that the relative position uncertainty is perfectly correlated in time. If there is any mis-modeling of the dynamics in the propagation of the relative position error covariance matrix, time-wise de-correlation of the uncertainty will increase the probability of collision over a given time interval. The paper gives some examples that illustrate this point. This paper argues that, for the present, Monte Carlo analysis is the best available tool for handling low-velocity encounters, and suggests some techniques for addressing the issues just described. One proposal is for the use of a non-parametric technique that is widely used in actuarial and medical studies. The other suggestion is that accurate process noise models be used in the Monte Carlo trials to which the non-parametric estimate is applied. A further contribution of this paper is a description of how the time-wise de-correlation of uncertainty increases the probability of collision.

*Aerospace Engineer, NASA Goddard Space Flight Center, Greenbelt, MD, 20771.

NOMENCLATURE

$\boldsymbol{R}_k, \boldsymbol{V}_k, \boldsymbol{X}_k$	Position, velocity, and position/velocity state vector of spacecraft $k = 1, 2$ relative to central body
$\boldsymbol{r}, \boldsymbol{v}, \boldsymbol{x}$	Position, velocity, and position/velocity state vector of spacecraft 2 relative to spacecraft 1, $\boldsymbol{r} = \boldsymbol{R}_2 - \boldsymbol{R}_1$, etc.
$\boldsymbol{f}(\boldsymbol{x}, t)$	Model of the unperturbed time evolution of $\boldsymbol{x}$, $\dot{\boldsymbol{x}}(t) = \boldsymbol{f}(\boldsymbol{x}, t)$
$\boldsymbol{w}(t)$	Hypothetical noise-like process perturbing the time evolution of $\boldsymbol{x}$ according to $\dot{\boldsymbol{x}}(t) = \boldsymbol{f}(\boldsymbol{x}, t) + B(t)\boldsymbol{w}(t)$
$\boldsymbol{e}$	Error in the relative state, $\boldsymbol{e} = \boldsymbol{x} - \mathrm{E}[\boldsymbol{x}]$
$P(t)$	Relative state error covariance matrix, $P(t) = \mathrm{E}[\boldsymbol{e}(t)\boldsymbol{e}(t)^{\mathrm{T}}]$
$P(t_i, t_j)$	Relative state error auto-covariance matrix, $P(t_i, t_j) = \mathrm{E}[\boldsymbol{e}(t_i)\boldsymbol{e}(t_j)^{\mathrm{T}}]$
$\Phi(t, t_i)$	State transition matrix for $\boldsymbol{e}$, $\dot{\Phi}(t, t_i) = A(t)\Phi(t, t_i), A(t) = \partial \boldsymbol{f}/\partial \boldsymbol{x}, \Phi(t_i, t_i) = I$
$Q(t), Q_d(t, t_i)$	Power spectral density of $\boldsymbol{w}(t)$, and process noise covariance, $Q_d(t, t_i) = \int_{t_i}^{t}\int_{t_i}^{t} \Phi(u, t_i)B(u)\mathrm{E}[\boldsymbol{w}(u)\boldsymbol{w}(s)^{\mathrm{T}}]B(s)^{\mathrm{T}}\Phi(s, t_i)^{\mathrm{T}}\mathrm{d}s\mathrm{d}u$
$\rho(\boldsymbol{r}, t)$	Probability density function of the relative position
$\mathbb{V}_i$	Convex set of points in $\mathbb{R}^3$ representing a protection volume surrounding the combined hard-body volumes of the two spacecraft, at a particular time, t_i
$p_c(t), p_{nc}(t)$	Instantaneous probability of collision, $p_c(t_i) = \Pr(\boldsymbol{r}(t_i) \in \mathbb{V}_i)$, and probability of not colliding, $p_{nc}(t_i) = \Pr(\boldsymbol{r}(t_i) \notin \mathbb{V}_i)$
$p_c(t, t_i), p_{nc}(t, t_i)$	Cumulative probability of collision, and probability of not colliding, over a time interval
$\Sigma(t, t_i)$	Auto-covariance of joint density associated with $p_{nc}(t, t_i)$
$s(t)$	Survivor function, $s(t) = \Pr(t_c > t)$, where t_c is the time of collision; is equal to $p_{nc}(t, t_i)$ for $t_i = 0$.

INTRODUCTION

The problem of estimating the probability of collision between an operational spacecraft and orbital debris has been widely studied. Foster and Estes[1] and Akella, et al.[2] describe the debris problem, and Chan's approximate analytical solution,[3] which is valid for cases in which the uncertainty in the relative positions is much larger than the combined hard-body radius, is now widely accepted. All of these methods assume that the encounter is brief, so that the relative motion may be assumed to be along a straight line normal to the encounter plane, and focus on the computation of the instantaneous probability of collision at the single moment of closest approach. Patera[4] describes one way to relax the "linear" motion assumption, and also accommodate time-varying uncertainty.

An implicit, but not necessarily obvious, assumption in all of these techniques is that the relative position uncertainty is perfectly correlated in time. If there is any mis-modeling of the dynamics in the propagation of the relative position error covariance matrix, time-wise de-correlation of the uncertainty will increase the probability of collision over a given time interval. Some examples given in the sequel illustrate this point. If the dynamics uncertainty can be accurately modeled as a Brownian motion diffusion process, the time-evolution of the

probability density of the relative position can be modeled by the Fokker-Planck Equation (FPE),

$$\frac{\partial \rho}{\partial t} = -\boldsymbol{f}(\boldsymbol{x},t)\frac{\partial \rho}{\partial \boldsymbol{x}} - \rho(\boldsymbol{x},t)\frac{\partial \boldsymbol{f}}{\partial \boldsymbol{x}} + \frac{1}{2}\mathrm{tr}Q(t)\frac{\partial^2 \rho}{\partial \boldsymbol{x}\partial \boldsymbol{x}} \tag{1}$$

The FPE however is very difficult to solve efficiently for systems of high dimensionality. The recent work of Kumar, et al.[5] has proposed the use of more efficient solution techniques, but this work has not yet achieved the goal of applying these techniques to a realistic space encounter.

In current practice, therefore, the Monte Carlo method is still widely used to study problems associated with low-velocity encounters. This approach is not without issues of its own. A question that is open to discussion is always how many Monte Carlo trials need to be run to assure adequate results. One way to address this question is to specify a confidence interval, based on the number of trials, but once again, the choice of confidence limits is left open to the analyst. A more subtle issue is right censoring, which is associated with the concept that one never knows if a particular trial would have ended in collision if the simulation were run a bit longer. A further issue with the Monte Carlo technique is that it is only as good as the accuracy of its inputs; uncertainties in the assumed error models will pollute the results. In this technique, the initial conditions are perturbed based on an initial covariance matrix. In an operational system, this covariance is typically the result of an orbit determination (OD) process. Whether or not the OD itself utilized process noise, the accuracy in predicting the resulting covariance matrix to a future epoch will be limited, and empirical techniques for the addition of process noise to these covariance propagations have been found to enhance the prediction accuracy.[6] The physical justification for adding process noise is that certain parameters in the dynamics model used for state and covariance propagation are not known to high precision. Therefore, the addition of diffusive uncertainty, which the process noise accomplishes, introduces a conservative bound on the resulting propagation errors, so long as the process noise covariance itself is accurate. Setting aside for the moment the issues of finding accurate initial covariance and process noise covariance, and whether or not white noise is the best way to model the dynamics uncertainty, there remains the issue that Monte Carlo analysis often does not introduce additional noise at each simulation step based on the process noise covariance. This omission would appear to be questionable, since without it, the propagations in the Monte Carlo trials will omit any uncertainty in the dynamics that is actually present.

This work takes the view that, for the present, Monte Carlo analysis is the best available tool for handling low-velocity encounters, and suggests some techniques for addressing the issues just described. One proposal is for the use of a non-parametric technique, known as the Kaplan-Meier estimator, that is widely used in the realm of actuarial and medical studies for handling the right censoring bias inherent in Monte Carlo trials. The other suggestion is that accurate process noise models be used in the Monte Carlo trials to which the non-parametric estimate is applied. A further contribution of this paper is a description of how the time-wise de-correlation of uncertainty increases the probability of collision.

The remainder of this paper is organized as follows. First, a fairly extensive background section describes the issues highlighted above, and illustrates the issues with two examples of increasing complexity. The next section describes a proposed procedure for forming non-

parametric estimates of the collision probability, and applies the procedure to the examples of the background section, as well as a somewhat realistic formation flying problem. The final section concludes, summarizes, and offers suggestions for further related work.

BACKGROUND

This section first derives the joint density associated with $p_{nc}(t, t_i)$ over a series of discrete sample points in order to show the effect of time-wise de-correlation on $p_c(t, t_i)$, due to the diffusive nature of process noise. It then illustrates this effect with two simplified examples of reduced dimensionality so that the geometry involved is evident. Next, a subsection describes some existing methods for determining accurate values for the initial error covariance and process noise covariance. The final subsection discusses some concepts from the actuarial and life sciences literature known as the hazard and survivor functions, and discusses their relevance to the problem of determining the probability of collision over an interval.

Joint Density

Considering a discrete series of time samples, the probability of collision over an interval of such samples, $p_c(t_n, t_0)$, is the probability associated with the union of the events that the perturbed relative positions, $\boldsymbol{r}_i$, are inside the volumes, $\mathbb{V}_i$, defining the protection region at each sample time t_i. This may be written as the complement of the probability of no collision, $p_{nc}(t_n, t_0)$, associated with the intersection of the events that the $\boldsymbol{r}_i$ are outside the protection regions,

$$p_c(t_n, t_0) = \Pr(\bigcup_{i=0}^{n} \boldsymbol{r}_i \in \mathbb{V}_i) \tag{2}$$

$$= 1 - \Pr(\bigcap_{i=0}^{n} \boldsymbol{r}_i \in \bar{\mathbb{V}}_i) \tag{3}$$

$$= 1 - p_{nc}(t_n, t_o), \tag{4}$$

where $\bar{\mathbb{V}}_i$ represents the complement of the set $\mathbb{V}_i$. Note that Eq. 2 is only an approximation, and unless a fairly dense sampling of time points are considered, Eq. 2 might underestimate $p_c(t_n, t_0)$ severely, since it could miss collisions that occur between the sample times.

With this caveat in mind, the joint probability that approximates the probability of not colliding over an interval is given by the integration of the joint density function $\rho(\boldsymbol{r}_n, \boldsymbol{r}_{n-1}, \cdots \boldsymbol{r}_1, \boldsymbol{r}_0, \Sigma)$ over each of the complements of the protection regions,

$$p_{nc}(t_n, t_0) = \iiint_{\bar{\mathbb{V}}_n} d\boldsymbol{r}_n \iiint_{\bar{\mathbb{V}}_{n-1}} d\boldsymbol{r}_{n-1} \cdots \iiint_{\bar{\mathbb{V}}_1} d\boldsymbol{r}_1 \iiint_{\bar{\mathbb{V}}_0} d\boldsymbol{r}_0 \rho(\boldsymbol{r}_n, \boldsymbol{r}_{n-1}, \cdots \boldsymbol{r}_1, \boldsymbol{r}_0, \Sigma), \tag{5}$$

where, assuming a Gaussian density, $\rho(\boldsymbol{r}_n, \boldsymbol{r}_{n-1}, \cdots \boldsymbol{r}_1, \boldsymbol{r}_0, \Sigma)$ is

$$\rho(\boldsymbol{r}_n, \boldsymbol{r}_{n-1}, \cdots \boldsymbol{r}_1, \boldsymbol{r}_0, \Sigma) = \frac{\exp\left(-\frac{1}{2}\left[\boldsymbol{e}_n^{\mathrm{T}}, \boldsymbol{e}_{n-1}^{\mathrm{T}}, \cdots \boldsymbol{e}_1^{\mathrm{T}}, \boldsymbol{e}_0^{\mathrm{T}}\right] \Sigma^{-1} \left[\boldsymbol{e}_n, \boldsymbol{e}_{n-1}, \cdots \boldsymbol{e}_1, \boldsymbol{e}_0\right]\right)}{\sqrt{(2\pi)^{3(n+1)}|\Sigma|}} \tag{6}$$

and where $\boldsymbol{e}_i = \boldsymbol{r}_i - \mathrm{E}[\boldsymbol{r}_i]$ are the errors in the relative positions. The autocovariance of the relative position errors, Σ, is

$$\Sigma = \begin{bmatrix} P_{\boldsymbol{r}_n} & P_{\boldsymbol{r}_n\boldsymbol{r}_{n-1}} & \cdots & P_{\boldsymbol{r}_n\boldsymbol{r}_1} & P_{\boldsymbol{r}_n\boldsymbol{r}_0} \\ P_{\boldsymbol{r}_{n-1}\boldsymbol{r}_n} & P_{\boldsymbol{r}_{n-1}} & \cdots & P_{\boldsymbol{r}_{n-1}\boldsymbol{r}_1} & P_{\boldsymbol{r}_{n-1}\boldsymbol{r}_0} \\ \vdots & \vdots & \ddots & \vdots & \vdots \\ P_{\boldsymbol{r}_1\boldsymbol{r}_n} & P_{\boldsymbol{r}_1\boldsymbol{r}_{n-1}} & \cdots & P_{\boldsymbol{r}_1} & P_{\boldsymbol{r}_1\boldsymbol{r}_0} \\ P_{\boldsymbol{r}_0\boldsymbol{r}_n} & P_{\boldsymbol{r}_0\boldsymbol{r}_{n-1}} & \cdots & P_{\boldsymbol{r}_0\boldsymbol{r}_1} & P_{\boldsymbol{r}_0} \end{bmatrix}, \tag{7}$$

where the covariance of the relative position error generally includes a cross-covariance between the the errors in the satellites' absolute positions,

$$P_{\boldsymbol{r}_i} = P_{\boldsymbol{R}_1}(t_i) + P_{\boldsymbol{R}_2}(t_i) - P_{\boldsymbol{R}_1\boldsymbol{R}_2}(t_i) - P^{\mathrm{T}}_{\boldsymbol{R}_1\boldsymbol{R}_2}(t_i) \tag{8}$$

and the relative position autocovariance over a time interval is

$$\begin{aligned} P_{\boldsymbol{r}_i\boldsymbol{r}_j} &= \Phi_{\boldsymbol{r}}(t_i, t_j)P_j \\ &= \Phi_{\boldsymbol{r}}(t_i, t_0)P_0\Phi^{\mathrm{T}}_{\boldsymbol{r}}(t_j, t_0) + \sum_{k=j}^{i} \Phi_{\boldsymbol{r}}(t_i, t_k)Q_d(t_k, t_{k-1}). \end{aligned} \tag{9}$$

In Eq. 9, $\Phi_{\boldsymbol{r}}(t_i, t_j)$ denotes the upper three rows of the 6×6 state transition matrix, i.e., $[\Phi_{\boldsymbol{r}\boldsymbol{r}}(t_i, t_j), \Phi_{\boldsymbol{r}\boldsymbol{v}}(t_i, t_j)]$. Using Eq. 9, one may decompose the expression for Σ into a summation:

$$\begin{aligned} \Sigma = &\begin{bmatrix} \Phi_{\boldsymbol{r}}(t_n, t_0) \\ \Phi_{\boldsymbol{r}}(t_{n-1}, t_0) \\ \vdots \\ \Phi_{\boldsymbol{r}}(t_1, t_0) \\ I \end{bmatrix} P_0 \begin{bmatrix} \Phi_{\boldsymbol{r}}(t_n, t_0) \\ \Phi_{\boldsymbol{r}}(t_{n-1}, t_0) \\ \vdots \\ \Phi_{\boldsymbol{r}}(t_1, t_0) \\ I \end{bmatrix}^{\mathrm{T}} + \begin{bmatrix} \Phi_{\boldsymbol{r}}(t_n, t_1) \\ \vdots \\ \Phi_{\boldsymbol{r}}(t_2, t_1) \\ I \\ 0 \end{bmatrix} Q_d(t_1, t_0) \begin{bmatrix} \Phi_{\boldsymbol{r}}(t_n, t_1) \\ \vdots \\ \Phi_{\boldsymbol{r}}(t_2, t_1) \\ I \\ 0 \end{bmatrix}^{\mathrm{T}} \\ &+ \cdots + \begin{bmatrix} \Phi_{\boldsymbol{r}}(t_n, t_{n-1}) \\ I \\ 0 \\ \vdots \\ 0 \end{bmatrix} Q_d(t_{n-1}, t_{n-2}) \begin{bmatrix} \Phi_{\boldsymbol{r}}(t_n, t_{n-1}) \\ I \\ 0 \\ \vdots \\ 0 \end{bmatrix}^{\mathrm{T}} + \begin{bmatrix} I \\ 0 \\ \vdots \\ 0 \\ 0 \end{bmatrix} Q_d(t_n, t_{n-1}) \begin{bmatrix} I \\ 0 \\ \vdots \\ 0 \\ 0 \end{bmatrix}^{\mathrm{T}} \end{aligned} \tag{10}$$

Clearly, the evaluation of Eq. 5 poses challenges perhaps as great as the solution of the FPE, and at best, will only give an approximate result. It does however offer insight into the nature of the problem. Since the first term in Equation 10 has at most the rank of P_0, and each of the remaining terms have at most the rank of their corresponding $Q_d(t_i, t_{i-1})$, then it is clear that $|\Sigma| = 0$ if there is no process noise. This merely indicates that, given a realization of the random initial relative position, $\boldsymbol{r}_0$, the $\boldsymbol{r}_i$ are not random variables when there is no process noise. In this case, the initial distribution of the position errors completely determines $p_{nc}(t_n, t_0) = \Pr(\bigcap_{i=0}^{n} \boldsymbol{r}_i \in \bar{\mathbb{V}}_i)$. Thus, when there is no process noise, the joint probability that there are no collisions over a series of discrete sample times

reduces to the individual probability that the perturbed initial relative position does not lie within the region representing the combined mapping back to the initial time of the various protection regions at each sample time, that is,

$$p_{nc}(t_n, t_0) = \Pr(\bigcap_{i=0}^{n} \boldsymbol{r}_i \in \bar{\mathbb{V}}_i) = \Pr(\bigcap_{i=0}^{n} \boldsymbol{r}_0 \in g(\bar{\mathbb{V}}_0, \bar{\mathbb{V}}_1, ..., \bar{\mathbb{V}}_n)) \tag{11}$$

where g is the mapping of the protection regions to the initial time. Note that this mapping should be performed with the dynamics governing the PDF, which are not necessarily the same as the dynamics governing the time evolution of the protection regions (although typically they are the same for the satellite collision problem).

Effect of Time Correlation

Equation 10 illustrates two sources for time-wise de-correlation to arise. The first term in the summation shows that the uncertainty in initial conditions will evolve according to the system dynamics, which will induce a time-wise de-correlation on the order the time constant of the dynamics. The remaining terms in the summation show how the presence of process noise induces a persistent de-correlating effect. Figures 1 and 2 illustrate these points with a pair of examples. To simplify the illustration, these examples do not use realistic two-body orbital dynamics; a later example introduces more realistic two-body motion. From these examples, it is clear that time correlation can drastically affect the outcome, even when the instantaneous moments of the density are identical.

In the example Figure 1 illustrates, two spacecraft in circular orbits are initially separated by 2.5 deg in true anomaly, and drifting together at a rate of 1 deg per orbit period. This example only considers the along-track motion of the two spacecraft. At each point in time, there is a unit variance Gaussian distribution of the relative position errors. In each of the three subplots, a different time correlation holds. A ± 0.5 deg region represents the projection onto the approach path of a substantial protection region in excess of the combined hard-body radius, which fills a parallelogram when time is the horizontal axis, as in this figure. The dark circles impinging the protection region represent close approach violations.

In the example Figure 2 illustrates, a spacecraft orbits a neighboring circular orbit spacecraft in a plane inclined 30 deg to the local horizontal so that its relative motion is a circle, with radius 2.5 km. This example only considers the two-dimensional motion of the spacecraft in the orbital plane. As in the one-dimensional example, at each point in time, there is a unit variance Gaussian distribution of the relative position errors, and as before, in each of the three subplots, a different time correlation holds. A 1.5 km radius circular region represents the "protection region" in excess of the combined hard-body radius, which creates a spiral tunnel when time is the third axis, as in this figure. As before, the dark circles impinging the protection region represent close approach violations.

To further illustrate the effect on collision probability of changing the time correlation, Table 1 shows some results of directly evaluating the integrals of Eq. 5, for the one-dimensional example that Figure 1 shows. In order to make this calculation practical, the

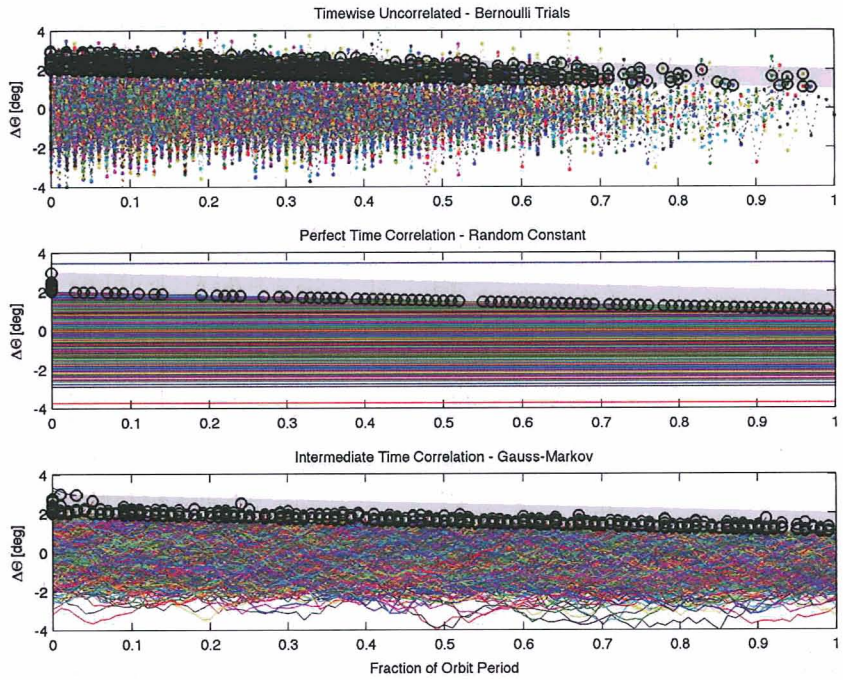

Figure 1: One-dimensional along-track approach trajectory example (1000 trials, 100 time increments).

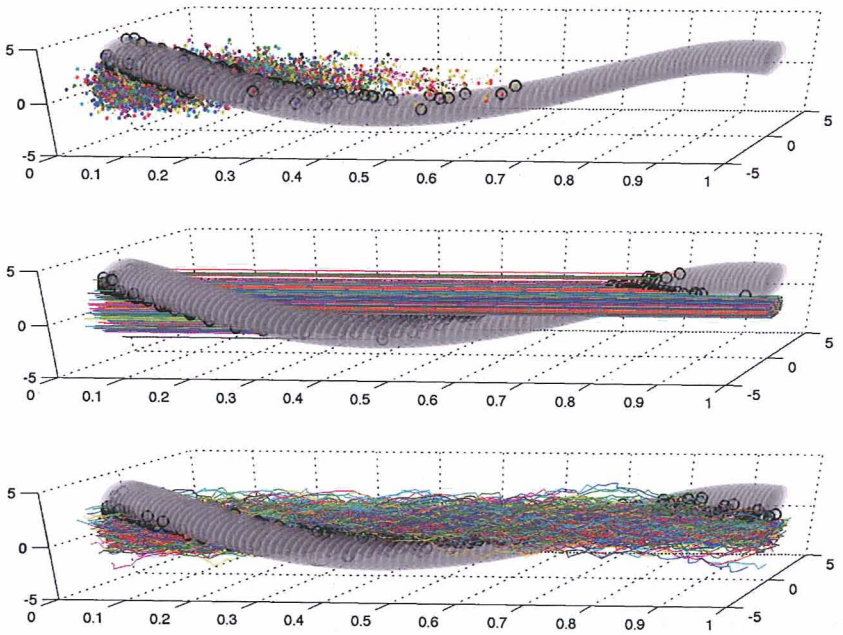

Figure 2: Two-dimensional circular relative motion example (1000 trials, 100 time increments).

number of time increments had to be reduced from 100 to 10 steps[2]. The table clearly shows that decreasing the time correlation substantially increases the probability of collision over the interval, for this example.

Table 1: Effect of changing correlation time (vs. baseline value of 0.3 sec), for the intermediate case from Figure 1, with ten (vs. 100) time increments.

Correlation Time [sec]	$p_{nc}(1,0)$	$p_c(1,0)$
0.01	0.412	0.588
0.03	0.416	0.584
0.1	0.489	0.521
0.3	0.611	0.389
1.0	0.740	0.260
3.0	0.805	0.195
10	0.834	0.166

Covariance Prediction

In order for any type of collision prediction to be accurate, there is a need to predict the covariance accurately, which requires an accurate process noise covariance. This process noise covariance need not be based on a white noise model, e.g. Wright's work on sequentially correlated process noise based on gravity mismodeling;[7] what matters is getting a good prediction. In some cases, empirical techniques, e.g. Duncan and Long,[6] are currently in use. An apparently little-known fact is that sequential smoothing techniques can provide optimal estimates of the process noise sequence. Appendix X of Bierman's text[8] shows the estimate for $\boldsymbol{w}(t)$. Recently, Psiaki described a sigma-point smoother[9] that also shows the update for the process noise and its covariance. In the usual sequential form of the Rausch-Tung-Striebel smoother, the process noise update takes the following form:

$$J_{ix} = \hat{P}_i \Phi_i^{\mathrm{T}} \bar{P}_{i+1}^{-1}, \tag{12}$$

$$J_{iw} = Q_{di} \bar{P}_{i+1}^{-1}, \tag{13}$$

$$x_i^* = \hat{x}_i + J_{ix}(x_{i+1}^* - \bar{x}_{i+1}), \tag{14}$$

$$w_i^* = J_{iw}(x_{i+1}^* - \bar{x}_{i+1}), \tag{15}$$

$$P_i^* = \hat{P}_i - J_{ix}(P_{i+1}^* - \bar{P}_{i+1}) J_{ix}^{\mathrm{T}}, \tag{16}$$

$$Q_{di}^* = Q_{di} - J_{iw}(P_{i+1}^* - \bar{P}_{i+1}) J_{iw}^{\mathrm{T}}, \tag{17}$$

where $\bar{(\cdot)}$, and $\hat{(\cdot)}$ denote the specified quantities just prior to, and after, the forward filter measurement update, respectively, and $(\cdot)^*$ denotes the backward smoother estimate. One should note that this technique does not directly provide Q_{di}, the forward filter process noise covariance, which is the parameter needed for accurate covariance prediction. However, the estimates it provides of the process noise sequence, w_i^*, may prove useful as part of the filter tuning process.

[2]One consequence of this large time step is that, for the smaller correlation times, it becomes increasingly likely for the Gauss-Markov model to take steps completely across the protection region between time steps; such steps are considered to be collisions.

Actuarial Analysis of Failure Times

A common problem in the fields of actuarial and medical studies is the determination of models for the time until some event, most often death, occurs. In these studies, there is typically a set of observations of the time of this event for a large group of individuals, and the analyst wishes to determine a distribution for these data. These data typically do not cover the entire lifespan of the individuals, so that many of the individuals are still surviving at the end of the data span. It may also occur that some individuals leave the study early, for reasons other than death. The literature refers to these conditions as *right censoring.* There are related concepts of *left censoring* and *left truncation.* In left censoring an individual failure occurs prior to some specific time, but the exact time of failure is unknown. In left truncation, an individual that would otherwise have been included in the study is not because they have already died prior to the beginning of the data span.

According to a standard textbook,[10] there are three specifications for the failure time distribution that are "particularly useful:" the survivor function, the probability density, and the hazard function. The survivor function, $s(t)$, is the probability that the time of the event in question is greater than some specified value, so it is the complement of the cumulative distribution function. The survivor function is particularly important because "the right tail [of the distribution] is the important component for the incorporation of right censoring." The hazard function is the "instantaneous rate at which failures occur for items that are surviving" at a given time, for continuous time models, and the "conditional probability of failure at [a specified time], given that the individual has survived to [the specified time]" for discrete-time models. General models for survival time can have both continuous and discrete components to the hazard function.

The optimal non-parametric estimate for the survivor function is found by maximizing a likelihood function on the space of all survivor functions. This is a discrete survivor function formed as the product of hazard components, $1 - h_i/r_i$, where h_i is the number of items that fail at each t_i, and r_i is the number of items remaining at risk for failure at t_i. Note that this assumes that the lifecycles of individuals are independent from each other, and that any censoring that occurs is independent, but does *not* assume independence between between time samples for a given individual, which the Bernoulli trials assumption often used in engineering failure analysis imposes. The result is known as the Kaplan-Meier or product limit estimator for the survivor function:

$$\hat{s}(t_j) = \prod_{i=1}^{j} \frac{r_i - h_i}{r_i} \tag{18}$$

Note that if there is no right censoring at any interior time samples (i.e. no one leaves the study prior to its completion), then $r_{i+1} = r_i - h_i$ so that the survivor function reduces to the intuitive value of $\hat{s}(t_j) = 1 - \sum_{i=1}^{j} h_i/m$, where m is the total number of individuals in the data set.

Applying the obvious relationships of these concepts to the satellite collision problem is the subject of the next section.

NON-PARAMETRIC ESTIMATE FOR $p_c(t_n, t_0)$

This section proposes a procedure based on the discussion above for computing collision probability over an interval, that addresses all of the issues mentioned previously. Next, it applies the procedure to the examples of the previous section, and somewhat more realistic example of a formation flying problem.

Proposed Procedure

Supposing that the Kaplan-Meier survivor estimate resulting from an accurately performed Monte Carlo study is a suitable proxy for the probability of not colliding over the interval of the Monte Carlo study,

$$p_c(t_n, t_0) = 1 - p_{nc}(t_n, t_0) = 1 - \Pr(t_c > t_n) = 1 - \hat{s}(t_n), \tag{19}$$

this paper suggests the following procedure for estimating the probability of not colliding over that interval, and hence an estimate of $p_c(t_n, t_0)$.

1. Obtain realistic estimates of both the initial covariance *and* the process noise covariance associated with the prediction model, via empirical techniques such as Duncan and Long[6] suggest, or via a smoother, such as the sigma-point smoother described by Psiaki.[9]

2. Perform a monte-carlo prediction study with m trials, using these realistic values for both the initial covariance and the process noise.

3. Compute the Kaplan-Meier estimate of the survivor function,[11] i.e. the probability that the time of collision is later than a given time:

$$\hat{s}(t_j) = \prod_{i=1}^{j} \frac{r_i - h_i}{r_i}, \tag{20}$$

   where r_i is number of trials at risk, i.e. those trials that have not resulted in a collision up to time t_j, (i.e. those trials that would be right censored if the trial ended at t_j), and h_i is the number of trials that have resulted in a collision at time t_j. Note that for most Monte Carlo studies, there should be no interior right censoring, so the survivor function will reduce to

$$\hat{s}(t_j) = 1 - \sum_{i=1}^{j} h_i/m. \tag{21}$$

4. Use Greenwood's formula[12] to compute the sample variance of $\hat{s}$:

$$\widehat{\mathrm{var}}[\hat{s}(t_j)] = \hat{s}(t_j)^2 \sum_{i=1}^{j} \frac{h_i}{r_i(r_i - h_i)}. \tag{22}$$

5. If $\hat{s}$ is near one (or zero), so that confidence limits based on the Greenwood sample variance exceed one (or zero), then use instead the technique suggested by Kalbfleish and Prentice:[10] compute

$$\hat{\xi}^2(t) = \widehat{\mathrm{var}}[\log \hat{s}(t)] / \log[\hat{s}(t)]^2, \tag{23}$$

which is the asymptotic variance of $\log[-\log \hat{s}(t)]$, and then for the confidence interval of $s(t)$ use

$$[\hat{s}(t)]^{\exp(\pm z_\alpha \hat{\xi}(t)}, \tag{24}$$

where z_α is the normal deviate corresponding to the desired confidence interval, e.g. $z_\alpha = 1.96$ for $1 - \alpha = 95\%$ confidence limits.

6. If $\hat{s}$ is exactly equal to one, then more trials are needed, since by conventional wisdom no system has immortal life. If running more trials is not practical, then an estimate, which is based on the binomial distribution, of the reliability that would correspond to $1 - \alpha$ two-sided confidence limits, with the right confidence interval having $\alpha/2$ of the mass resting solely at 100% reliability, is given by

$$\hat{p}_{nc} = \exp(\log(\alpha/2)/m), \tag{25}$$

(the left confidence interval may be found from the binomial cumulative density evaluated at $\alpha/2$, or via the normal approximation to the binomial density via the usual method.)

7. If the confidence limits are larger than desired, run more trials. Note that the equation above may be solved for m to specify the number of trials required to establish a given reliability, with given confidence bounds, if the given reliability is close to one.

Results for Constant Density Examples

Figures 5 and 6 illustrate the results of applying the procedure outlined above for the simplified examples that Figures 1 and 2 show. In addition, Figure 7 shows the results of applying the procedure to a simple three-dimensional example (circular relative motion trajectory test case, with $R = \sigma = 1$ and $r = 0.3$) that Reference 4 describes.

For the one- and two-dimensional perfect time correlation cases, it is possible to compute the exact value of $p_c(t_n, t_0)$, since the mapping of the protection region described in Eq. 11 is simply the projection of these regions onto the $t = 0$ plane; in other words, it is the shadow cast by the protection regions back onto $t = 0$, as Figures 3 and 4 show. In Figure 3, the shadow of the two-dimensional protection region onto $t = 0$ is one-dimensional, and the third dimension shows the constant probability density. In Figure 4, the shadow of the three-dimensional protection region onto $t = 0$ is a two-dimensional annulus, and it is not possible to show the probability density, as this would require a fourth dimension. These figures illustrate the point made by Eq. 11 and its accompanying text.

For these cases, the shadows cast especially simple geometries. In Figure 3 the shadow projects onto one of the tails of the normal density that governs the initial error distribution, so that computing p_c reduces to evaluating the cumulative normal density over the portion of the tail outlined in Figure 3. In Figure 4, the shadow is a disk with a missing center, so that computing p_c reduces to computing the circular error probable, or the cumulative Rayleigh distribution over the outer disk, and then subtracting the Rayleigh mass contained in the inner disk, or hole. It is convenient to find these probabilities by evaluation of the

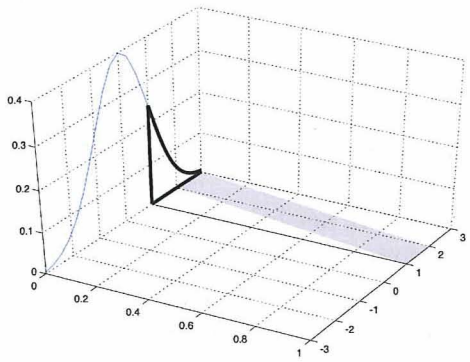

Figure 3: Shadow cast on $t = 0$ plane by motion of protection region in Figure 1

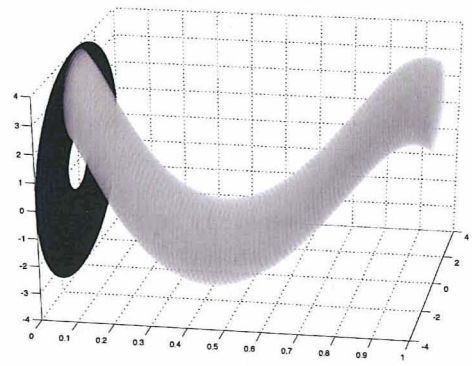

Figure 4: Shadow cast on $t = 0$ plane by motion of protection region in Figure 2

χ^2 density, with ν degrees of freedom,

$$m_{\chi^2}(z,\nu) = \int_0^z \frac{z^{(\nu-2)/2}\mathrm{e}^{-z/2}}{2^{\nu/2}\Gamma(\nu/2)}\mathrm{d}z, \tag{26}$$

since this density generalizes the symmetric Gaussian density to arbitrary dimensionality. For the one-dimensional example ($\nu = 1$),

$$p_{nc}(1,0) = 1 - p_c(1,0) = 1 - \frac{m_{\chi^2}(3^2,1) - m_{\chi^2}(1,1)}{2} = 0.843, \tag{27}$$

where the integral must be halved since only one tail is needed, and for the two-dimensional example ($\nu = 2$),

$$p_{nc}(1,0) = 1 - p_c(1,0) = 1 - m_{\chi^2}(4^2,2) - m_{\chi^2}(1,2) = 0.394. \tag{28}$$

For the three-dimensional example, Reference 4 gives the following result for the exact collision probability for the perfect time correlation case:

$$p_c(t,t_i) = \frac{2}{\sigma}\sqrt{\frac{2}{\pi}}\exp\left[\frac{-(R^2+r^2)}{2\sigma^2}\right]\int_0^r \sinh\left(\frac{R\sqrt{r^2-x^2}}{\sigma^2}\right)\mathrm{d}x, \tag{29}$$

$$p_c(1,0) = \frac{2}{(1)}\sqrt{\frac{2}{\pi}}\exp\left[\frac{-(1^2+0.3^2)}{2(1)^2}\right]\int_0^{0.3} \sinh\left(\frac{(1)\sqrt{0.3^2-x^2}}{(1)^2}\right)\mathrm{d}x = 0.066146, \tag{30}$$

$$p_{nc}(1,0) = 1 - p_c(1,0) = 0.934. \tag{31}$$

The figures show that the proposed procedure estimates the known probability for the perfect correlation cases to within the confidence limits. For intermediate and zero correlations, the procedure produces the expected reductions in the survival probability.

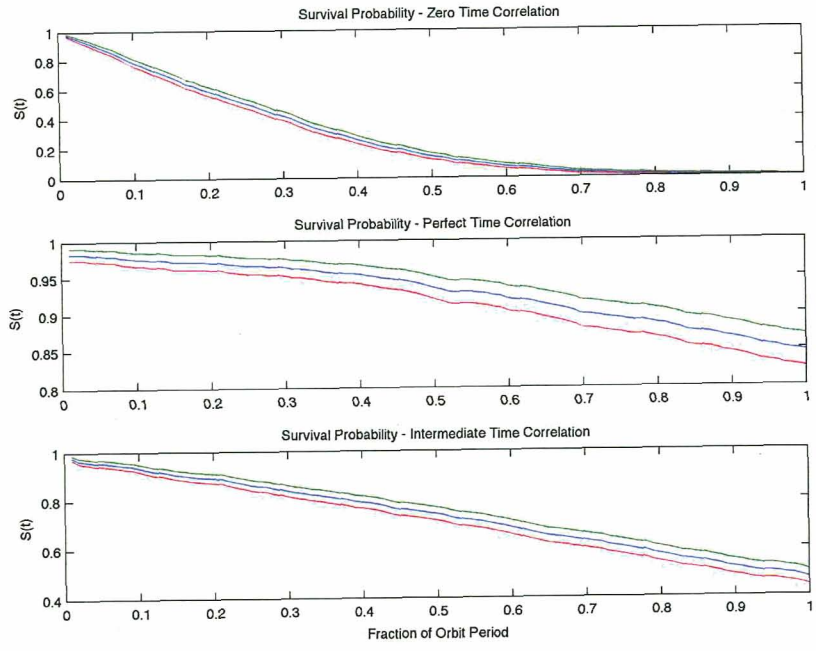

Figure 5: The empirical survival probability (blue), with ±95% confidence interval (red and green), for the one-dimensional case Figure 1 shows. For the perfect time correlation case, the exact value after one orbit period is 0.843.

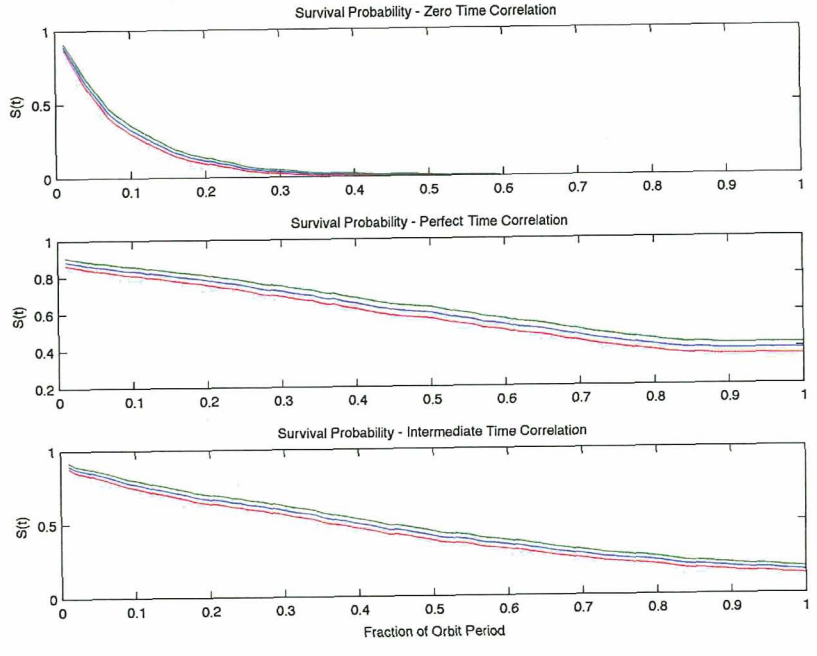

Figure 6: The empirical survival probability (blue), with ±95% confidence interval (red and green), for the two-dimensional case Figure 2 shows. For the perfect time correlation case, the exact value after one orbit period is 0.394.

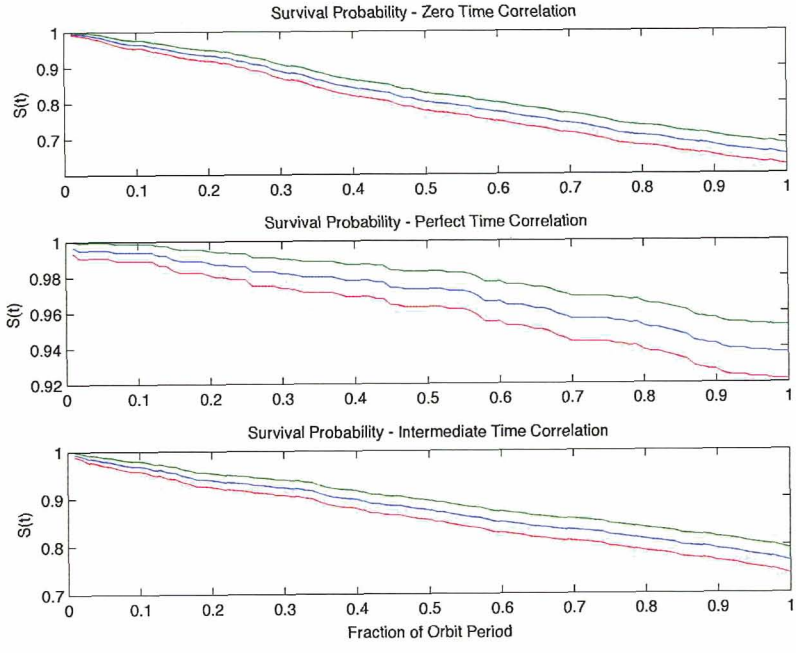

Figure 7: The empirical survival probability(blue), with $\pm 95\%$ confidence interval (red and green), for the three-dimensional case Reference 4 describes (1000 trials, 100 time increments). For the perfect time correlation case, the exact value after one orbit period is 0.9339.

Results for a Realistic Formation Flying Example

Figures 8 and 9 shows a somewhat realistic three-dimensional formation flying example. A spacecraft orbits a neighboring circular orbit spacecraft in the neighbor's orbit plane, so that its relative motion is a 2×1 ellipse, with semi-major axis 200 m. There is uncertainty in both the initial relative position and velocity (1 m and 1 mm/sec, 1σ, respectively, with $-.95$ correlation coefficient between radius and speed, and between radial velocity and in-track position), as well as acceleration process noise of 3 milligee/sec$^{1/2}$. The protection region is a 50 m sphere. The example is only partially realistic, since it assumes two-body gravity, and the process noise is artificial white noise. In reality, the process noise arises due to mis-modeling of the dynamics. Figure 9 shows an expected step decrease in the survival probability each time the relative trajectory crosses the orbit of the reference spacecraft.

CONCLUSIONS

This paper has proposed a procedure for computing the collision probability over an interval using a non-parametric technique, known as the Kaplan-Meier estimator, that is widely used in the realm of actuarial and medical studies. The estimator accommodates the right censoring bias inherent in Monte Carlo trials. This proposal will only be as good as the fidelity of the Monte Carlo procedure, and this paper has offered some suggestions to improve the accuracy of the process noise and initial covariance matrices used in the Monte Carlo trials to which the non-parametric estimate is applied. This paper has also described how the time-wise de-correlation of uncertainty due to process noise increases the probability of collision.

Although other techniques have been proposed for low-velocity encounters that are less costly to perform than Monte Carlo analysis, unless there is sufficient justification for ignoring uncertainties in the propagation model, the use of any technique that does not properly model time-wise de-correlation due to the model errors would not appear to be advisable. One possible avenue for future work that could address this problem might be to generalize works such as Reference 4 so as to perform a four-dimensional integration over space and time. This would be analogous to integration over the volume of the spiral tube that Figure 2 illustrates, but generalized to a hyper-tube through three spatial axes perpendicular to the time axis. Alternatively, continued progress in the numerical solution of the FPE may offer the best hope for efficiently solving this difficult problem.

ACKNOWLEDGMENTS

Discussions with the following individuals have shaped the development of this work: Landis Markley, Terry Alfriend, Conrad Schiff, Marco Concha, Mrinal Kumar, John Junkins, Mark Psiaki, and Carol Moore.

REFERENCES

1. J. L. Foster, Jr. and H. S. Estes, "A Parametric Analysis of Orbital Debris Collision Probability and Maneuver Rate for Space Vehicles," Tech. Rep. JSC–25898, NASA Johnson Space Center, Houston, TX, 1992.

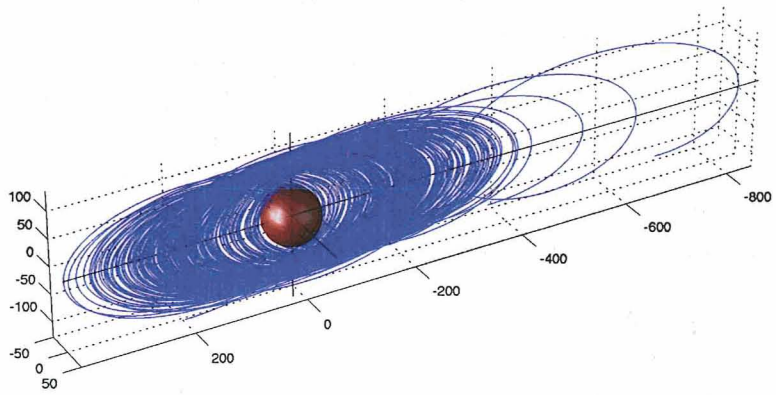

Figure 8: Three-dimensional in-plane relative motion example (100 trials).

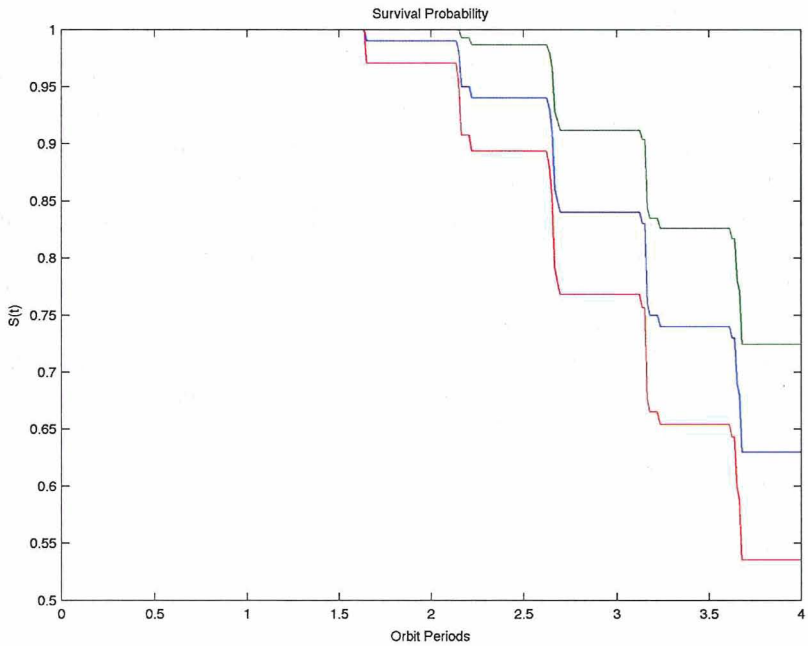

Figure 9: The empirical survival probability (blue), with ±95% confidence interval (red and green), for the three-dimensional case Figure 8 shows (100 trials). Each of the step decreases in $s(t)$ occurs when the relative trajectory crosses the orbit path of the reference spacecraft.

2. M. R. Akella and K. T. Alfriend, "Probability of Collision Between Space Objects," *Journal of Guidance, Control and Dynamics*, Vol. 23, No. 5, September–October 2000, pp. 769–772.

3. K. Chan, "Improved Analytical Expressions for Computing Spacecraft Collision Probabilities," *Space Flight Mechanics 2003*, Univelt, 2003.

4. R. P. Patera, "Satellite Collision Probability for Nonlinear Relative Motion," *Journal of Guidance, Control, and Dynamics*, Vol. 26, No. 5, September–October 2003, pp. 728–733.

5. M. Kumar, P. Singla, S. Chakravorty, and J. L. Junkins, "The Partition of Unity Finite Element Approach to the Stationary Fokker-Planck Equation," *Astrodynamics 2006*, Advances in the Astronautical Sciences, Univelt, 2006.

6. M. Duncan and A. Long, "Realistic Covariance Prediction for the Earth Science Constellation," *Astrodynamics 2006*, Advances in the Astronautical Sciences, Univelt, 2006.

7. J. R. Wright, "Sequential Orbit Determination with Auto-Correlated Gravity Modeling Errors," *Journal of Guidance and Control*, Vol. 4, No. 3, May–June 1980, pp. 304–309.

8. G. J. Bierman, *Factorization Methods for Discrete Sequential Estimation*, Academic Press, New York, 1977.

9. M. L. Psiaki, "Derivation and Simulation Testing of a Sigma-Points Smoother," *Proceedings of the AIAA Guidance, Navigation, and Control Conference (to appear in Journal of Guidance Control and Dynamics)*, 2006.

10. J. D. Kalbfleisch and R. L. Prentice, *The Statistical Analysis of Failure Data*, Wiley, New York, 1980.

11. E. L. Kaplan and P. Meier, "Non-Parametric Estimation from Incomplete Observations," *Journal of the American Statistical Society*, Vol. 53, 1958, pp. 457–481.

12. M. Greenwood, "A Report on the Natural Duration of Cancer, Appendix I: The 'Errors of Sampling' of the Survivorship Tables," *Journal of the Royal Statistical Society*, Vol. 33, 1926, pp. 1–26.